NANO LETTERS

Letter

pubs.acs.org/NanoLett

Two-Phase Electrochemical Lithiation in Amorphous Silicon

Jiang Wei Wang,[†,⊥] Yu He,[‡,⊥] Feifei Fan,[§] Xiao Hua Liu,[∥] Shuman Xia,[§] Yang Liu,[∥] C. Thomas Harris,[∥] Hong Li,[*,‡] Jian Yu Huang,[∥] Scott X. Mao,[*,†] and Ting Zhu[*,§]

[†]Department of Mechanical Engineering and Materials Science, University of Pittsburgh, Pittsburgh, Pennsylvania 15261, United States

[‡]Beijing National Laboratory for Condensed Matter Physics, Institute of Physics, Chinese Academy of Sciences, Beijing 100190, People's Republic of China

[§]Woodruff School of Mechanical Engineering, Georgia Institute of Technology, Atlanta, Georgia 30332, United States

[∥]Center for Integrated Nanotechnologies (CINT), Sandia National Laboratories, Albuquerque, New Mexico 87185, United States

Supporting Information

ABSTRACT: Lithium-ion batteries have revolutionized portable electronics and will be a key to electrifying transport vehicles and delivering renewable electricity. Amorphous silicon (*a*-Si) is being intensively studied as a high-capacity anode material for next-generation lithium-ion batteries. Its lithiation has been widely thought to occur through a single-phase mechanism with gentle Li profiles, thus offering a significant potential for mitigating pulverization and capacity fade. Here, we discover a surprising two-phase process of electrochemical lithiation in *a*-Si by using *in situ* transmission electron microscopy. The lithiation occurs by the movement of a sharp phase boundary between the *a*-Si reactant and an amorphous Li_xSi (*a*-Li_xSi, $x \sim 2.5$) product. Such a striking amorphous−amorphous interface exists until the remaining *a*-Si is consumed. Then a second step of lithiation sets in without a visible interface, resulting in the final product of *a*-Li_xSi ($x \sim 3.75$). We show that the two-phase lithiation can be the fundamental mechanism underpinning the anomalous morphological change of microfabricated *a*-Si electrodes, i.e., from a disk shape to a dome shape. Our results represent a significant step toward the understanding of the electrochemically driven reaction and degradation in amorphous materials, which is critical to the development of microstructurally stable electrodes for high-performance lithium-ion batteries.

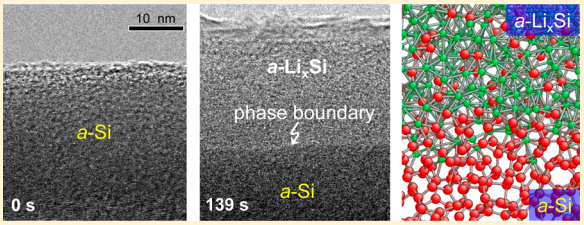

KEYWORDS: *Amorphous silicon, two-phase lithiation, amorphous−amorphous interface, lithium-ion battery, in situ transmission electron microscopy*

Silicon is an attractive high-capacity anode material for Li-ion batteries.[1−7] However, insertion of Li into Si causes large volume expansion of ~280% at the full capacity ($Li_{3.75}Si$) at room temperature. The issue of volume expansion is particularly significant in Si electrodes that have been often fabricated from crystalline Si (*c*-Si). This is because lithiation of *c*-Si occurs through a two-phase mechanism, i.e., growth of amorphous Li_xSi (*a*-Li_xSi, $x \sim 3.75$) separated from *c*-Si by a sharp phase boundary.[8−12] A large change of Li concentration across this amorphous−crystalline interface (ACI) of about 1 nm in width can cause drastically inhomogeneous volume expansion, leading to high stress, pulverization, and capacity loss.[8,13−16]

To mitigate the degradation associated with the two-phase lithiation in *c*-Si, considerable efforts have been devoted to its amorphous counterpart,[17−23] which is intuitively thought to eliminate two-phase regions, resulting in a continuous Li reaction and homogeneous volume expansion. However, whether lithiation of amorphous Si (*a*-Si) occurs by a single-phase or two-phase mechanism remains unclear.[24−27] A further interest in this question arises from the experiment reported in this paper which reveals anomalous shape changes during the electrochemical lithiation of patterned *a*-Si disk electrodes.

To clearly resolve how *a*-Si is lithiated, we conduct *in situ* experiment of electrochemical lithiation inside a transmission electron microscope (TEM). Real-time visualization of the first lithiation process directly reveals a two-phase mechanism that occurs by movement of a sharp phase boundary between the *a*-Si reactant and an *a*-Li_xSi ($x \sim 2.5$) product. It is unexpected to observe such an amorphous−amorphous interface (AAI), which has been rarely seen in the literature of solid-state phase transformations.[28−31] Unique to the lithiation of *a*-Si, there exists an abrupt change of Li concentration across the phase boundary that renders a marked contrast in electron transparency between the two coexisting amorphous phases, thereby facilitating the discovery of the AAI through *in situ* TEM. Upon the completion of two-phase lithiation, a second step of lithiation occurs in *a*-Li_xSi ($x \sim 2.5$) without a visible

Received: November 28, 2012
Revised: January 12, 2013
Published: January 16, 2013

   dx.doi.org/10.1021/nl304379k | *Nano Lett.* 2013, 13, 709−715

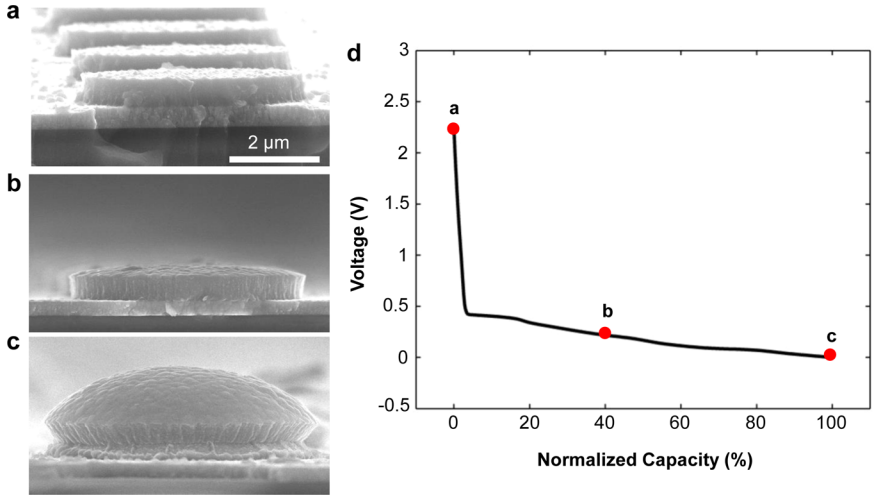

Figure 1. Anomalous shape growth of electrochemically lithiated amorphous Si electrodes.[21] (a) SEM image of as-fabricated *a*-Si disk electrodes. (b) An intermediate state of a representative disk electrode during electrochemical lithiation. (c) A fully lithiated disk electrode exhibiting the domelike shape. (d) Normalized voltage versus lithiation capacity. A full lithiation corresponds to the formation of *a*-$Li_{3.75}Si$. Red dots indicate the states shown in the SEM images of (a–c).

interface, resulting in the final product of *a*-Li_xSi ($x \sim 3.75$) with a total volume expansion of about 280%. Nevertheless, the predominance of two-phase lithiation appears to be the key to anomalous shape growth in microfabricated *a*-Si electrodes, as shown by our chemomechanical modeling.

Results and Discussion. *Anomalous Growth of a-Si Disk Electrodes.* Figure 1 shows the anomalous shape changes of a patterned *a*-Si electrode during electrochemical lithiation. The as-fabricated electrode consisted of an array of equally spaced circular microdisks on a titanium (Ti)-coated quartz substrate, as revealed by the scanning electron microscope (SEM) image in Figure 1a. Each of the disks had a thickness of 500 nm and a diameter of 5 μm, and the distance between the neighboring disks was also 5 μm. The Raman spectra indicate that as-prepared Si disks were amorphous (Figure S1). Electrochemical lithiation was conducted with the patterned *a*-Si electrode, and SEM images were taken to follow the morphological evolution during various stages of lithiation (Figures 1b,c). Figure 1d shows the normalized voltage profile during the first lithiation, in which the red dots marked as "a" through "c" correspond to the SEM images shown in Figures 1a–c, respectively. The growth of the *a*-Si disk electrodes upon lithiation was highly anisotropic, with the vertical expansion dominating the lateral one. The most striking shape change was the anomalous nonuniform expansion; namely, the vertical expansion of the disk electrode increased markedly with decreasing radial distance, resulting in a final dome shape at the conclusion of lithiation. From both SEM imaging and atomic force microscope (AFM) measurement, we estimate the volume expansion around 280%, confirming an approximately full lithiation to *a*-$Li_{3.75}Si$ (He et al.[21]). In addition, the base of the lithiated disk electrode expanded by ~20% in the radial direction, which is suggestive of the occurrence of interfacial sliding or plastic flow in the metallic substrate for accommodating the radial growth.[22,23]

Two-Phase Mechanism in a-Si Revealed by in Situ Electrochemical Lithiation. To understand the formation of the dome shape, we directly visualized how *a*-Si was lithiated with *in situ* electrochemical lithiation experiments inside a TEM. As schematically shown in Figure S2, a nanobattery was constructed in the half-cell configuration.[32,33] The working electrode was an individual carbon nanofiber coated with an *a*-Si surface layer, denoted as *a*-Si/CNF. Figures 2a–c show the TEM image and electron diffraction pattern of *a*-Si/CNF before lithiation. The CNF was hollow, with both the outer and inner surfaces covered with *a*-Si (Figure 2a). Figure 2b shows a high-magnification TEM image of the surface *a*-Si layer before lithiation. This *a*-Si layer was disordered, with a thickness of about 20 nm. On the surface of the *a*-Si layer, a thin layer of amorphous carbon (3 nm thick) was coated to serve as a fast path for Li^+ ion and electron transport in the longitudinal direction of the system. Beneath the *a*-Si layer, the CNF exhibited a pattern of layered graphitic sheets. The electron diffraction pattern of *a*-Si/CNF (Figure 2c) confirms that the Si layer is amorphous. Upon lithiation, Li^+ ions first diffused along the fast paths, i.e., the surface of *a*-Si and the interface between *a*-Si and CNF, and then diffused into the bulk of the *a*-Si layer along the radial direction. This sequential process resulted in a sandwiched mode of lithiation in *a*-Si,[27] as shown in Figure S3. To highlight the essential physical process, we hereafter focus on the *in situ* high-resolution TEM characterization of two-phase lithiation in the surface *a*-Si layer.

Figures 2d–f and the video in the Supporting Information show the dynamic propagation of an individual AAI, which initiated near the surface and moved toward the center of CNF. The pristine *a*-Si surface layer on the CNF was initially about 21 nm (Figure 2d). Upon lithiation, Li^+ ions consumed Si atoms by forming an *a*-Li_xSi alloy, and a sharp phase boundary formed between the *a*-Si and *a*-Li_xSi layer. As the phase boundary propagated, the lithiated layer was markedly thickened and the *a*-Si layer was gradually depleted (Figures 2e,f). Figure 2g shows the thickness versus time in *a*-Si and *a*-Li_xSi. The velocity of the AAI is approximately constant (0.06 nm/s), which indicates that the lithiation reaction at the phase boundary is the rate-limiting step.[34] Assuming cylindrical symmetry, we estimate the volume increase in the *a*-Li_xSi layer relative to its pristine state, as shown in Figure 2h. This result, along with *in situ* testing of several other *a*-Si/CNFs (Figures S4a–c and S5a–c), suggests the average value of x to be about 2.5 in the *a*-Li_xSi phase (corresponding to volume expansion ~170%, ref 35). While the TEM contrast was inadequate for resolving the Li distribution in the *a*-Li_xSi layer,

dx.doi.org/10.1021/nl304379k | *Nano Lett.* 2013, 13, 709–715

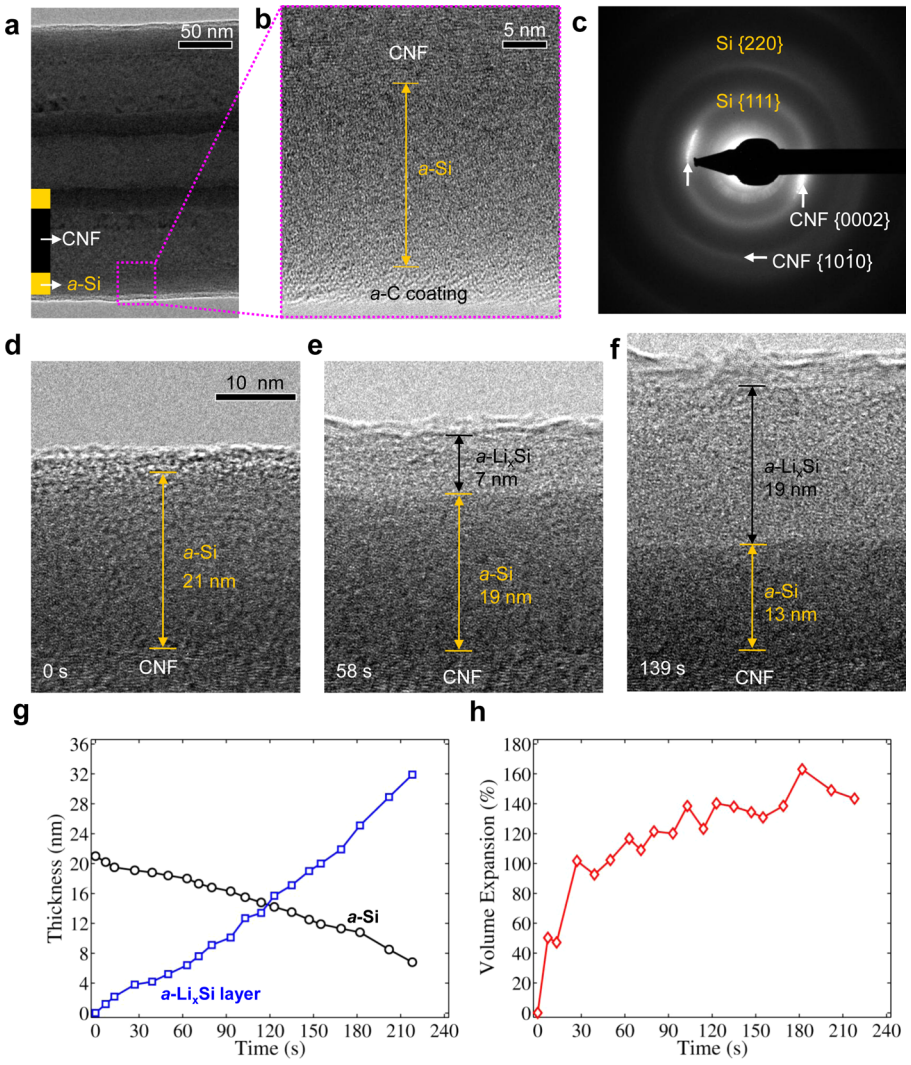

Figure 2. A sharp phase boundary observed during *in situ* electrochemical lithiation of amorphous Si coated on a carbon nanofiber. (a–c) Pristine *a*-Si/CNF. The CNF is hollow, with both the outer and inner surfaces covered with *a*-Si. The *a*-Si coating layer is about 20 nm thick, and it is covered with an amorphous carbon layer of 3 nm thick. The high-resolution TEM image (b) and electron diffraction pattern (c) indicate that the Si coating layer is amorphous. The yellow arrows in (b) indicate the interface between *a*-Si and CNF. (d–f) Time-elapse high-resolution TEM images showing the migration of a phase boundary between *a*-Si and *a*-Li$_x$Si. The *a*-Li$_x$Si layer in (f) grew to 19 nm thick and had a lighter contrast than the underneath *a*-Si, whose thickness decreased from 21 nm (shown in (d)) to 13 nm. (g) Thickness versus time in *a*-Si and *a*-Li$_x$Si, and (h) the associated volume increase in the *a*-Li$_x$Si layer.

we performed the digital image correlation (DIC) analysis to quantitatively determine the spatial distribution of lithiation-induced strains from TEM images. As detailed in the Supporting Information, our DIC results show that (1) the Li diffusion-induced strain is negligibly small in the *a*-Li$_x$Si layer as the *a*-Si/*a*-Li$_x$Si phase boundary moves and (2) the local phase-transformation-induced strain is about 160% in the region swept by the *a*-Si/*a*-Li$_x$Si phase boundary. These results indicate that the lithiation-induced expansion dominantly occurs at the *a*-Si/*a*-Li$_x$Si phase boundary, and the Li concentration gradient is negligibly small in the lithiated layer of *a*-Li$_x$Si ($x \sim 2.5$). It is worth noting that the localized lithiation could be accelerated due to the high dosage rate of electron beam exposure required by high-resolution TEM imaging (Figure S6). This is in contrast with the extended lithiation through the propagation of a long and straight phase boundary under the beam-blank or low-resolution imaging conditions. Nevertheless, the observation of sharp phase boundaries remained the same and reproducible in all the TEM experiments (Figure 2 and Figures S3–S6), clearly showing that the two-phase mechanism dominates in the electrochemical lithiation of *a*-Si. In addition, *in situ* TEM observation shows that the two-phase boundary exists until the remaining *a*-Si is consumed. This is followed by a second step of lithiation in *a*-Li$_x$Si ($x \sim 2.5$) without a visible interface, resulting in the final product of *a*-Li$_x$Si ($x \sim 3.75$) with a total volume expansion of ~280%, as shown in Figures S4d and S5d. This step of lithiation proceeded extremely fast, and we were not able to acquire a series of high-quality TEM images. Hence, unlike the first step of lithiation, the strain field could not be quantified by the DIC analysis for determining Li distributions. Future studies are needed with a better control of the second-step lithiation in *a*-Si in order to clarify whether it occurs by a single-phase or two-phase reaction.

The above *in situ* TEM experiment reveals an unexpected two-phase process of electrochemical lithiation in *a*-Si. To understand why the two-phase mechanism dominates the single-phase one in the first step of lithiation, we recall that the

dx.doi.org/10.1021/nl304379k | *Nano Lett.* 2013, 13, 709–715

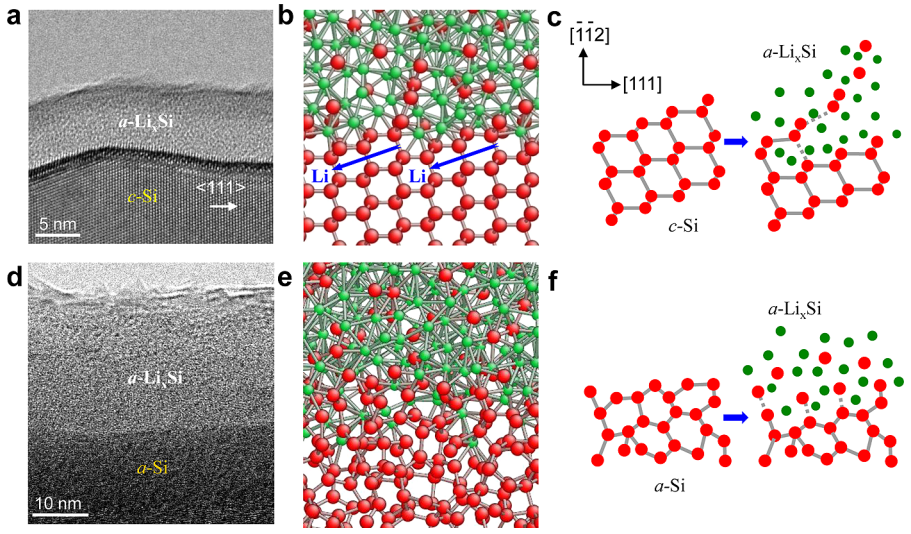

Figure 3. Comparison of the two-phase lithiation mechanism in *c*-Si and *a*-Si. (a) A high-resolution TEM image showing a sharp phase boundary between the reactant of *c*-Si and the product of *a*-Li$_x$Si.[11] (b) A snapshot from molecular dynamics simulation showing the atomic structures near the amorphous−crystal phase boundary.[11] The Li concentration is locally high near the surface of *c*-Si (red) and a group of Li atoms (green) collectively weaken the strong Si−Si covalent bonding, thereby facilitating the dissolution of Si atom from *c*-Si surface, as schematically shown in (c). (d) A high-resolution TEM image showing a sharp phase boundary between *a*-Si and *a*-Li$_x$Si ($x \sim 2.5$). (e) A snapshot from molecular dynamics simulation showing the atomic structures near the amorphous−amorphous interface. The *a*-Si consists of a continuous random network of Si atoms. Similar to (b), the Li concentration is locally high near the surface of *a*-Si. (f) Schematics showing the proposed mechanism of dissolution of Si atoms from the *a*-Si surface into *a*-Li$_x$Si alloy.

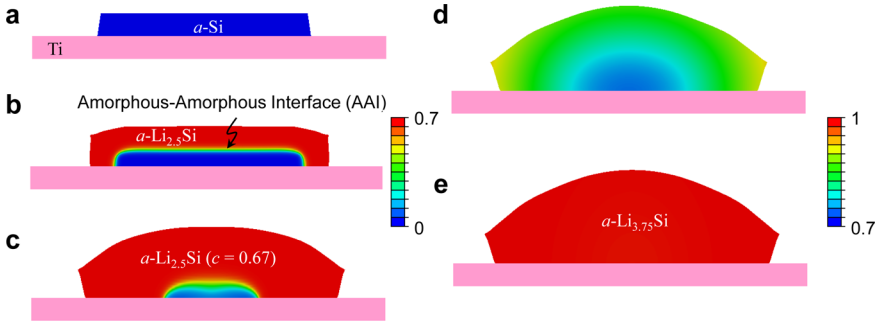

Figure 4. Chemomechanical simulation of lithiation-induced morphological evolution in an *a*-Si disk electrode. (a−c) The first step of two-phase lithiation to form *a*-Li$_{2.5}$Si, showing both the Li profile and shape growth: (a) a pristine *a*-Si electrode on a Ti substrate; (b) an intermediate state, showing the simulated amorphous−amorphous interface (AAI); and (c) a state close to the final *a*-Li$_{2.5}$Si. A drastic change of Li concentration occurs across the sharp AAI between *a*-Si and *a*-Li$_{2.5}$Si. Note that the remaining *a*-Si electrode undergoes a marked shrinkage in the radial direction. Contour indicates the normalized Li concentration of *c*; *a*-Si and *a*-Li$_{2.5}$Si correspond to c = 0 and 0.67, respectively. (d, e) The second step of single-phase lithiation to form *a*-Li$_{3.75}$Si: (d) an intermediate state, showing the smooth and gentle Li distribution; and (e) the final state of *a*-Li$_{3.75}$Si. To display the gradual change of Li concentrations in (d, e), a color map different from (a−c) is used, with *a*-Li$_{3.7.5}$Si corresponding to c = 1.

linear time dependence of thickening of *a*-Li$_x$Si (Figure 2g) indicates that the reaction at the amorphous−amorphous interface is the rate-limiting step. The disruption of a covalent Si network, either crystalline or amorphous, is generally known to be difficult. This is because of the strong covalent Si−Si bonding; e.g., the energy needed to remove a Si atom from the *c*-Si surface has been measured to be a large fraction of the formation energy of a vacancy (2.4−3.5 eV, ref 36), resulting in a low rate of Si dissociation from the Si network at room temperature. Incidentally, our recent *in situ* high-resolution TEM experiment has revealed a two-phase lithiation mechanism of *c*-Si to *a*-Li$_x$Si through the movement of a sharp amorphous−crystalline interface (Figure 3a), facilitated by layer-by-layer ledge flow at the *c*-Si surface.[11] While the atomic structure of *a*-Si lacks the long-range order, it consists of a continuous random network of Si atoms. The local bonding environment in *a*-Si is similar to that of *c*-Si (Figures 3b,e), in the sense that both *a*-Si and *c*-Si involve the strong, directional Si bonding with a small number of miscoordinated/over-coordinated defects. As a result, in both cases the local Li concentration near the phase boundary should be high in the Li-rich *a*-Li$_x$Si phase, so as to facilitate an interfacial process of several Li atoms enclosing a single Si or a Si−Si pair at the surface of *c*-Si or *a*-Si,[37,38] as illustrated in Figures 3c,f. The previous study of silicide formation indicates that a group of metallic atoms (Li in this case) can collectively weaken the Si−Si covalent bonding by electron transfer.[36] Hence, the Li "flocking" at the amorphous−amorphous phase boundary is expected to lead to easy dissociation of the Si atom from the covalently bonded *a*-Si (Figure 3f), facilitating the lithiation process at room temperature.

On the basis of the newly discovered two-phase lithiation in *a*-Si, our continuum chemomechanical simulation readily produced a dome shape during lithiation of the *a*-Si disk

dx.doi.org/10.1021/nl304379k | *Nano Lett.* 2013, 13, 709−715

electrode shown in Figure 1c. Figures 4a–c show the snapshots of simulated Li distributions and associated shape changes in a disk electrode undergoing two-phase lithiation. These results suggest two dominant factors that control the dome shape growth. First, the sharp phase boundary between *a*-Si and *a*-Li_xSi ($x \sim 2.5$) is responsible for anisotropic swelling by effectively promoting the vertical expansion while suppressing the lateral expansion. This arises from the drastic change of Li concentration across the phase boundary. That is, in order to minimize the strain mismatch between the unlithiated and lithiated phase, the lithiation strain occurring at the phase boundary tends to align with the local normal direction of the phase boundary. Note that the disk electrode in our experiment features a large aspect ratio between diameter and height, so that the majority of the phase boundary is parallel to the substrate, as shown in Figure 4b. As a result, the lithiation-induced expansion occurs dominantly in the vertical direction. In addition, assuming a finite shear strength against interfacial sliding between the disk electrode and substrate,[22,23] our simulations capture the radial expansion of about 20%, as measured from the experiment.

Second, the decreasing diameter of the unlithiated *a*-Si disk dictates the dome shape growth. Figures 4a–c show that as lithiation proceeds, the diameter of the unlithiated *a*-Si disk decreases, due to simultaneous in-flow of Li from both the top and side surfaces. This leads to a progressive decrease of the area of the phase boundary that is parallel to the substrate. The vertical expansion occurs mostly at this part of phase boundary with reducing area and thus gradually focuses onto the center of the disk electrode. As a result, the dome shape develops, featuring a markedly increased vertical expansion with decreasing radial distance to the disk center. It should be noted that the second step of lithiation, either by a single-phase or two-phase reaction, will not qualitatively change the final result of formation of a dome shape in the lithiated disk electrode. For example, we simulated the second step of lithiation from *a*-$Li_{2.5}Si$ to *a*-$Li_{3.75}Si$ by assuming a single-phase reaction with gentle Li profiles. As shown in Figure 4d,e, the electrode with an already dome shape further expands in a nearly self-similar manner, giving a final volume expansion of ~280% at the conclusion of lithiation to *a*-$Li_{3.75}Si$.

Finally, we note that while the anomalous shape growth in the microfabricated *a*-Si electrode is rationalized in terms of the effects of two-phase lithiation, its origin requires further study regarding the influence of the lithiation stress on Li diffusion, reaction, and deformation. At this point we cannot exclude the possibility that the dome shape would arise from the single-phase lithiation with gentle Li profiles, owing to the volume expansion mediated by the lithiation stress. However, we note that the redox peaks can be clearly seen in the cyclic voltammogram or dQ/dV (where Q is charge and V is voltage) curve for the *a*-Si thin film electrode (Figure S7). Similar redox peaks in *a*-Si are also reported in the literature.[39,40] The redox peak has been often correlated to the two-phase reaction. The first redox peak in Figure S7 likely results from the two-phase reaction between *a*-Si and *a*-Li_xSi ($x \sim 2.5$), and the second peak could be related to the transition from *a*-$Li_{2.5}Si$ to *a*-$Li_{3.75}Si$. The redox peaks therefore lend a support to the two-phase reaction mechanism. Moreover, our chemo-mechanical simulations indicate that the stress effect on shape growth should be secondary compared to the two-phase mechanism of lithiation (Figure S8 shows a typical simulation result of single-phase lithiation). Nevertheless, the experiment of microfabricated *a*-Si disk electrodes motivated the *in situ* TEM study, leading to a discovery of the two-phase electrochemical lithiation in amorphous electrodes.

Conclusions. We have discovered an unexpected two-phase lithiation mechanism in amorphous silicon through *in situ* TEM experiment. Such lithiation mechanism is in stark contrast to the widely believed single-phase mechanism in amorphous metals and alloys. The occurrence of a sharp amorphous–amorphous interface during electrochemical lithiation is attributed to the need for a high local Li concentration at the phase boundary so as for it to break the Si atom away from the covalently bonded *a*-Si. The two-phase lithiation can cause the anomalous morphological change of microfabricated amorphous silicon electrodes. Our work represents an important advance in the fundamental understanding of the working mechanisms of the high-capacity, amorphous electrodes in lithium-ion batteries.[41,42] Broadly, the demonstrated capability of *in situ* visualization of the amorphous–amorphous phase boundary opens new opportunities for the study of polyamorphism in amorphous materials.[28−31]

Methods. *Ex Situ Electrochemical Test of the Patterned a-Si Electrode.* An array of *a*-Si disk electrodes was made from a uniform *a*-Si thin film on a Ti-coated quartz substrate with the optical lithography and reactive ion etching (RIE) techniques, as described in detail in our previous work.[21] The *a*-Si thin film was deposited by radio-frequency sputtering of a pure Si (>99.999%) target with the sputtering power of 60 W. Before deposition, the vacuum chamber was evacuated to a pressure of 5.0×10^{-5} Pa and then was kept at 4 mTorr under high-purity argon (99.999%) ambient during deposition. The substrate was 500 nm thick Ti deposited on quartz by dc magnetron sputtering of a pure Ti (>99.999%) target. The S1813 (Shipley Co.) photoresist was spin-coated onto the as-prepared *a*-Si electrode and prebaked at 115 °C for 60 s. The exposure was carried out by an ultraviolet mask aligner system (Karl SussMA6, Germany). A PlasmaLab 80 plus RIE system (Oxford Instruments Company, UK) was used to transfer the resist patterns to the Si film. Reactive etching was conducted in SF_6–O_2 plasmon containing 30 standard cubic centimeter (sccm) SF_6 and 5 sccm O_2 at 100 mTorr for 2 min at 200 W radio-frequency power. The as-prepared, patterned *a*-Si electrode was analyzed with Raman spectroscopy with a Renishaw 1000NR spectrometer using an argon ion laser (wavelength λ = 514 nm). Spectra were collected in the wavenumber range of 200–1000 cm^{-1} with a resolution of 1 cm^{-1}.

To conduct the electrochemical test, a two-electrode cell was constructed with the patterned *a*-Si electrode as the working electrode and a Li foil as the counter electrode. The electrolyte was 1 M $LiPF_6$ dissolved in ethylene carbonate and dimethyl carbonate with a volumetric ratio of 1:1 (Shanghai Topsol Ltd., H_2O < 10 ppm). The cell was discharged at a constant current density of 5 $\mu A\ cm^{-2}$. *Ex situ* AFM experiments were performed using an AFM workstation (Nano Scope III_a, Bruker AXS) housed in an argon-purged glovebag. Contact mode was used in these *ex situ* AFM experiments. The AFM probe used to image the surface was silicon nitride Veeco probe (OTR8-35). The sample was opened in the glovebag without exposure to air. *Ex situ* SEM experiments were performed by a Hitachi-4800 microscope equipped with a sample transfer box, which permitted the transfer of air-sensitive samples from the glovebox into the SEM vacuum chamber without exposure to air. Before fixing the sample to the SEM holder, each electrode

dx.doi.org/10.1021/nl304379k | *Nano Lett.* 2013, 13, 709–715

was washed with anhydrous dimethyl carbonate and dried in the vacuum chamber in the glovebox.

In Situ Electrochemical Test of a-Si. The *a*-Si/CNF composite samples were prepared by coating *a*-Si onto CNFs with the chemical vapor deposition method (Applied Sciences Inc.). The *a*-Si coating was about 20 nm. In a typical *in situ* TEM experiment of electrochemical lithiation, the *a*-Si/CNF composite nanowires were glued to an aluminum (Al) rod with conductive silver epoxy, which served as the working electrode. Fresh Li metal was scratched off from a freshly cut surface of bulk Li with a tungsten (W) rod in a glovebox filled with helium (H_2O and O_2 concentration below 1 ppm), which served as the counter electrode and Li source. The two electrodes were mounted onto a Nanofactory TEM−scanning tunneling microscopy (STM) holder in a glovebox, which was transferred with a sealed plastic bag filled with dry helium and loaded into the TEM column. The Li metal was exposed to the air for about 2−5 s during the holder loading process. A native Li_2O layer was formed on the surface of Li metal, which served as the solid-state electrolyte to only conduct Li^+ ions. Inside the TEM, the Li_2O/Li terminal was driven by a piezo positioner to touch the *a*-Si/CNF-Al terminal. Once the contact was established, a negative bias (such as −2 V) was applied to the *a*-Si/CNF electrode to initiate the electrochemical lithiation. Both beam blank and *in situ* experiments were conducted to observe phase boundaries between the *a*-Si reactant and the *a*-Li_xSi product created during lithiation.

Modeling. We first simulate the two-phase lithiation that results in *a*-$Li_{2.5}Si$. The evolution of phase and microstructure is modeled by the nonlinear diffusion of Li, as described in detail in our recent work.[8,13] In finite element simulations of Li diffusion, the disk electrode is initially pristine and subjected to a constant Li flux I_0 at the surface. The normalized Li concentration behind the reaction front can quickly attain the high value (around $c = 0.67$, corresponding to *a*-$Li_{2.5}Si$), while that ahead of the front remains nearly zero. This produces a sharp reaction front, consistent with the experiment observation. To describe the lithiation-induced deformation, we adopt an elastic and perfectly plastic model.[8,13] The total strain rate, $\dot{\varepsilon}_{ij}$, is a sum of three contributions: $\dot{\varepsilon}_{ij} = \dot{\varepsilon}^c_{ij} + \dot{\varepsilon}^e_{ij} + \dot{\varepsilon}^p_{ij}$. Here, $\dot{\varepsilon}^e_{ij}$ and $\dot{\varepsilon}^p_{ij}$ denote the elastic and plastic strain rate, respectively; $\dot{\varepsilon}^c_{ij}$ denotes the chemical strain rate caused by lithiation and is proportional to the rate of the normalized Li concentration, $\dot{c}$. That is, $\dot{\varepsilon}^c_{ij} = \beta_{ij}\dot{c}$, where β_{ij} is the coefficient of lithiation-induced volume expansion. We assume that the outer surface of the disk electrode is traction free, and the interface shear strength is constant between the electrode and rigid substrate. We also test the case of an elastic−perfectly plastic substrate with a perfectly bonded interface. The two interface conditions give nearly indistinguishable results of the final dome shape, though the detailed distributions of shear stresses near the interface are slightly different. The above diffusion and elastic−perfectly plastic model is numerically implemented in the finite element package ABAQUS.[8,13] We also simulate the second step of single-phase lithiation that forms *a*-$Li_{3.75}Si$. In contrast to the aforementioned two-phase lithiation, we employ a constant diffusivity, giving a gentle variation of Li profiles. The axis-symmetric condition is used to reduce the computational cost. We choose the volume expansion parameters to be $\beta_{11} = \beta_{22} = \beta_{33} = 0.56$, giving the total volume increase of 280% for *a*-$Li_{3.75}Si$; the yield stress $\sigma_Y = 0.03E$, where E is Young's modulus, and Poisson's ratio $\nu = 0.3$. To understand the atomic structure near the phase boundary, we performed molecular dynamics (MD) simulations by using the reactive force field. The detailed procedures have been described in our previous work.[11,35]

■ ASSOCIATED CONTENT

Ⓢ Supporting Information

A video from *in situ* high-resolution TEM imaging, showing the two-phase electrochemical lithiation of *a*-Si, along with the digital image correlation (DIC) analysis of TEM images; additional figures of experiment and modeling. This material is available free of charge via the Internet at http://pubs.acs.org.

■ AUTHOR INFORMATION

Corresponding Author

*E-mail: ting.zhu@me.gatech.edu (T.Z.); sxm2@pitt.edu (S.X.M.); hli@iphy.ac.cn (H.L.).

Author Contributions

⊥These authors contributed equally to this work.

Notes

The authors declare no competing financial interest.

■ ACKNOWLEDGMENTS

We thank David Burton from Applied Sciences Inc. for providing the *a*-Si/CNF samples. S.X.M. acknowledges the NSF grant CMMI 08010934 through University of Pittsburgh and Sandia National Lab support. T.Z. acknowledges the support by the NSF Grant CMMI 1100205. This work was performed, in part, at the Center for Integrated Nanotechnologies, a US Department of Energy, Office of Basic Energy Sciences user facility. Sandia National Laboratories is a multiprogram laboratory managed and operated by Sandia Corporation, a wholly owned subsidiary of Lockheed Martin Company, for the U.S. Department of Energy's National Nuclear Security Administration under Contract DE-AC04-94AL85000. The research done at the Institute of Physics, Chinese Academy of Sciences, is supported by CAS project (KJCX2-YW-W26) and 973 project (2012CB932900).

■ REFERENCES

(1) Tarascon, J. M.; Armand, M. *Nature* **2001**, *414* (6861), 359−367.
(2) Goodenough, J. B.; Kim, Y. *Chem. Mater.* **2010**, *22* (3), 587−603.
(3) Li, H.; Huang, X. J.; Chen, L. Q.; Wu, Z. G.; Liang, Y. *Electrochem. Solid-State Lett.* **1999**, *2* (11), 547−549.
(4) Beaulieu, L. Y.; Eberman, K. W.; Turner, R. L.; Krause, L. J.; Dahn, J. R. *Electrochem. Solid-State Lett.* **2001**, *4* (9), A137−A140.
(5) Limthongkul, P.; Jang, Y. I.; Dudney, N. J.; Chiang, Y. M. *Acta Mater.* **2003**, *51* (4), 1103−1113.
(6) Chan, C. K.; Peng, H. L.; Liu, G.; McIlwrath, K.; Zhang, X. F.; Huggins, R. A.; Cui, Y. *Nat. Nanotechnol.* **2008**, *3* (1), 31−35.
(7) Magasinski, A.; Dixon, P.; Hertzberg, B.; Kvit, A.; Ayala, J.; Yushin, G. *Nat. Mater.* **2010**, *9* (4), 353−358.
(8) Liu, X. H.; Zheng, H.; Zhong, L.; Huang, S.; Karki, K.; Zhang, L. Q.; Liu, Y.; Kushima, A.; Liang, W. T.; Wang, J. W.; Cho, J.-H.; Epstein, E.; Dayeh, S. A.; Picraux, S. T.; Zhu, T.; Li, J.; Sullivan, J. P.; Cumings, J.; Wang, C.; Mao, S. X.; Ye, Z. Z.; Zhang, S.; Huang, J. Y. *Nano Lett.* **2011**, *11* (8), 3312−3318.
(9) Goldman, J. L.; Long, B. R.; Gewirth, A. A.; Nuzzo, R. G. *Adv. Funct. Mater.* **2011**, *21* (13), 2412−2422.
(10) Lee, S. W.; McDowell, M. T.; Choi, J. W.; Cui, Y. *Nano Lett.* **2011**, *11* (7), 3034−3039.
(11) Liu, X. H.; Wang, J. W.; Huang, S.; Fan, F.; Huang, X.; Liu, Y.; Krylyuk, S.; Yoo, J.; Dayeh, S. A.; Davydov, A. V.; Mao, S. X.; Picraux, S. T.; Zhang, S.; Li, J.; Zhu, T.; Huang, J. Y. *Nat. Nanotechnol.* **2012**, *7* (11), 749−756.

(12) McDowell, M. T.; Ryu, I.; Lee, S. W.; Wang, C.; Nix, W. D.; Cui, Y. *Adv. Mater.* **2012**, *24* (45), 6034−6041.
(13) Liu, X. H.; Zhong, L.; Huang, S.; Mao, S. X.; Zhu, T.; Huang, J. Y. *ACS Nano* **2012**, *6* (2), 1522−1531.
(14) Lee, S. W.; McDowell, M. T.; Berla, L. A.; Nix, W. D.; Cui, Y. *Proc. Natl. Acad. Sci. U. S. A.* **2012**, *109* (11), 4080−4085.
(15) Zhao, K. J.; Pharr, M.; Wan, Q.; Wang, W. L.; Kaxiras, E.; Vlassak, J. J.; Suo, Z. G. *J. Electrochem. Soc.* **2012**, *159* (3), A238−A243.
(16) Liu, X. H.; Fan, F.; Yang, H.; Zhang, S.; Huang, J. Y.; Zhu, T. *ACS Nano* **2013**, DOI: 10.1021/nn305282d.
(17) Beaulieu, L. Y.; Hatchard, T. D.; Bonakdarpour, A.; Fleischauer, M. D.; Dahn, J. R. *J. Electrochem. Soc.* **2003**, *150* (11), A1457−A1464.
(18) Hatchard, T. D.; Dahn, J. R. *J. Electrochem. Soc.* **2004**, *151* (6), A838−A842.
(19) Kasavajjula, U.; Wang, C. S.; Appleby, A. J. *J. Power Sources* **2007**, *163* (2), 1003−1039.
(20) Cui, L. F.; Ruffo, R.; Chan, C. K.; Peng, H. L.; Cui, Y. *Nano Lett.* **2009**, *9* (1), 491−495.
(21) He, Y.; Yu, X.; Li, G.; Wang, R.; Li, H.; Wang, Y.; Gao, H.; Huang, X. *J. Power Sources* **2012**, *216*, 131−138.
(22) Soni, S. K.; Sheldon, B. W.; Xiao, X. C.; Verbrugge, M. W.; Ahn, D.; Haftbaradaran, H.; Gao, H. J. *J. Electrochem. Soc.* **2012**, *159* (1), A38−A43.
(23) Haftbaradaran, H.; Xiao, X. C.; Verbrugge, M. W.; Gao, H. J. *J. Power Sources* **2012**, *206*, 357−366.
(24) Liao, H. W.; Karki, K.; Zhang, Y.; Cumings, J.; Wang, Y. H. *Adv. Mater.* **2011**, *23* (37), 4318−4322.
(25) Ghassemi, H.; Au, M.; Chen, N.; Heiden, P. A.; Yassar, R. S. *ACS Nano* **2011**, *5* (10), 7805−7811.
(26) Wang, C. M.; Li, X. L.; Wang, Z. G.; Xu, W.; Liu, J.; Gao, F.; Kovarik, L.; Zhang, J. G.; Howe, J.; Burton, D. J.; Liu, Z. Y.; Xiao, X. C.; Thevuthasan, S.; Baer, D. R. *Nano Lett.* **2012**, *12* (3), 1624−1632.
(27) Wang, J. W.; Liu, X. H.; Zhao, K.; Palmer, A.; Patten, E.; Burton, D.; Mao, S. X.; Suo, Z.; Huang, J. Y. *ACS Nano* **2012**, *6* (10), 9158−9167.
(28) Johnson, W. L. *Prog. Mater. Sci.* **1986**, *30* (2), 81−134.
(29) Mishima, O.; Takemura, K.; Aoki, K. *Science* **1991**, *254* (5030), 406−408.
(30) McMillan, P. F. *J. Mater. Chem.* **2004**, *14* (10), 1506−1512.
(31) Sheng, H. W.; Liu, H. Z.; Cheng, Y. Q.; Wen, J.; Lee, P. L.; Luo, W. K.; Shastri, S. D.; Ma, E. *Nat. Mater.* **2007**, *6* (3), 192−197.
(32) Huang, J. Y.; Zhong, L.; Wang, C. M.; Sullivan, J. P.; Xu, W.; Zhang, L. Q.; Mao, S. X.; Hudak, N. S.; Liu, X. H.; Subramanian, A.; Fan, H. Y.; Qi, L. A.; Kushima, A.; Li, J. *Science* **2010**, *330* (6010), 1515−1520.
(33) Liu, X. H.; Liu, Y.; Kushima, A.; Zhang, S. L.; Zhu, T.; Li, J.; Huang, J. Y. *Adv. Energy Mater.* **2012**, *2* (7), 722−741.
(34) Weichert, K.; Sigle, W.; van Aken, P. A.; Jamnik, J.; Zhu, C. B.; Amin, R.; Acarturk, T.; Starke, U.; Maier, J. *J. Am. Chem. Soc.* **2012**, *134* (6), 2988−2992.
(35) Huang, S.; Zhu, T. *J. Power Sources* **2011**, *196* (7), 3664−3668.
(36) Tu, K. N. *Appl. Phys. Lett.* **1975**, *27* (4), 221−224.
(37) Key, B.; Bhattacharyya, R.; Morcrette, M.; Seznec, V.; Tarascon, J. M.; Grey, C. P. *J. Am. Chem. Soc.* **2009**, *131* (26), 9239−9249.
(38) Key, B.; Morcrette, M.; Tarascon, J. M.; Grey, C. P. *J. Am. Chem. Soc.* **2011**, *133* (3), 503−512.
(39) Bourderau, S.; Brousse, T.; Schleich, D. M. *J. Power Sources* **1999**, *81*, 233−236.
(40) Wang, Y. H.; He, Y.; Xiao, R. J.; Li, H.; Aifantis, K. E.; Huang, X. J. *J. Power Sources* **2012**, *202*, 236−245.
(41) Scrosati, B.; Garche, J. *J. Power Sources* **2010**, *195* (9), 2419−2430.
(42) Dunn, B.; Kamath, H.; Tarascon, J. M. *Science* **2011**, *334* (6058), 928−935.